Measurement and resonance analysis of the ^{237}Np neutron capture cross section

C. Guerrero,[1,2] D. Cano-Ott,[1] E. Mendoza,[1] U. Abbondanno,[3] G. Aerts,[4] F. Álvarez-Velarde,[1] S. Andriamonje,[4] J. Andrzejewski,[5] P. Assimakopoulos,[6] L. Audouin,[7] G. Badurek,[8] P. Baumann,[9] F. Becvár,[10] F. Belloni,[3] E. Berthoumieux,[4] F. Calviño,[11] M. Calviani,[12,13] R. Capote,[14,15] C. Carrapiço,[16,4] A. Carrillo de Albornoz,[16] P. Cennini,[2] V. Chepel,[17] E. Chiaveri,[2] N. Colonna,[18] G. Cortes,[19] A. Couture,[20] J. Cox,[20] M. Dahlfors,[2] S. David,[7] I. Dillmann,[21] R. Dolfini,[22] C. Domingo-Pardo,[23] W. Dridi,[4] I. Duran,[24] C. Eleftheriadis,[25] M. Embid-Segura,[1] L. Ferrant,[7] A. Ferrari,[2] R. Ferreira-Marques,[17] L. Fitzpatrick,[2] H. Frais-Koelbl,[26] K. Fujii,[3] W. Furman,[27] I. Goncalves,[16] E. González-Romero,[1] A. Goverdovski,[28] F. Gramegna,[12] E. Griesmayer,[26] F. Gunsing,[4] B. Haas,[29] R. Haight,[30] M. Heil,[21] A. Herrera-Martinez,[2] M. Igashira,[31] S. Isaev,[4] E. Jericha,[8] F. Käppeler,[21] Y. Kadi,[2] D. Karadimos,[6] D. Karamanis,[6] V. Ketlerov,[28,2] M. Kerveno,[9] P. Koehler,[32] V. Konovalov,[27,2] E. Kossionides,[33] M. Krtička,[10] C. Lampoudis,[25,4] H. Leeb,[8] A. Lindote,[17] I. Lopes,[17] R. Lossito,[2] M. Lozano,[15] S. Lukic,[9] J. Marganiec,[5] L. Marques,[16] S. Marrone,[18] T. Martínez,[1] C. Massimi,[34] P. Mastinu,[12] A. Mengoni,[14,2] P. M. Milazzo,[3] C. Moreau,[3] M. Mosconi,[21] F. Neves,[17] H. Oberhummer,[8] S. O'Brien,[20] M. Oshima,[35] J. Pancin,[4] C. Papachristodoulou,[6] C. Papadopoulos,[36] C. Paradela,[24] N. Patronis,[6] A. Pavlik,[37] P. Pavlopoulos,[38] L. Perrot,[4] M. T. Pigni,[8] R. Plag,[21] A. Plompen,[39] A. Plukis,[4] A. Poch,[19] J. Praena,[12] C. Pretel,[19] J. Quesada,[15] T. Rauscher,[40] R. Reifarth,[30] M. Rosetti,[41] C. Rubbia,[22] G. Rudolf,[9] P. Rullhusen,[39] J. Salgado,[16] C. Santos,[16] L. Sarchiapone,[2] I. Savvidis,[25] C. Stephan,[7] G. Tagliente,[18] J. L. Tain,[23] L. Tassan-Got,[7] L. Tavora,[16] R. Terlizzi,[18] G. Vannini,[34] P. Vaz,[16] A. Ventura,[41] D. Villamarin,[1] M. C. Vicente,[1] V. Vlachoudis,[2] R. Vlastou,[36] F. Voss,[21] S. Walter,[21] H. Wendler,[2] M. Wiescher,[20] and K. Wisshak[21]

(n_TOF Collaboration)

[1]*CIEMAT, Centro de Investigaciones Energeticas Medioambientales y Tecnologicas, E-Madrid, Spain*

[2]*CERN, CH-Geneva, Switzerland*

[3]*Istituto Nazionale di Fisica Nucleare, I-Trieste, Italy*

[4]*CEA/Saclay–IRFU, F-Gif-sur-Yvette, France*

[5]*University of Lodz, PL-Lodz, Poland*

[6]*University of Ioannina, GR-Ioannina, Greece*

[7]*Centre National de la Recherche Scientifique/IN2P3–IPN, F-Orsay, France*

[8]*Atominstitut der Österreichischen Universitäten, Technische Universität Wien, A-Wien, Austria*

[9]*Centre National de la Recherche Scientifique/IN2P3–IReS, F-Strasbourg, France*

[10]*Charles University, CZ-Prague, Czech Republic*

[11]*Universidad Politecnica de Madrid, E-Madrid, Spain*

[12]*Istituto Nazionale di Fisica Nucleare, Laboratori Nazionali di Legnaro, I-35020 Legnaro, Italy*

[13]*Dipartimento di Fisica, Università di Padova, I-35122 Padova, Italy*

[14]*International Atomic Energy Agency (IAEA), Nuclear Data Section, A-1400 Vienna, Austria*

[15]*Universidad de Sevilla, E-41004 Sevilla, Spain*

[16]*Instituto Tecnológico e Nuclear (ITN), P-Lisbon, Portugal*

[17]*LIP - Coimbra & Departamento de Fisica da Universidade de Coimbra, P-Coimbra, Portugal*

[18]*Istituto Nazionale di Fisica Nucleare, I-Bari, Italy*

[19]*Universitat Politecnica de Catalunya, E-Barcelona, Spain*

[20]*University of Notre Dame, Notre Dame, Indiana 46556, USA*

[21]*Karlsruhe Institute of Technology (KIT), Institut für Kernphysik, D-Karlsruhe, Germany*

[22]*Università degli Studi Pavia, I-Pavia, Italy*

[23]*Instituto de Física Corpuscular, CSIC-Universidad de Valencia, E-Valencia, Spain*

[24]*Universidade de Santiago de Compostela, E-Santiago de Compostela, Spain*

[25]*Aristotle University of Thessaloniki, GR-Thessaloniki, Greece*

[26]*Fachhochschule Wiener Neustadt, A-Wiener Neustadt, Austria*

[27]*Joint Institute for Nuclear Research, Frank Laboratory of Neutron Physics, Dubna, Russia*

[28]*Institute of Physics and Power Engineering, Kaluga region, Obninsk, Russia*

[29]*Centre National de la Recherche Scientifique/IN2P3–CENBG, F-Bordeaux, France*

[30]*Los Alamos National Laboratory, Los Alamos, New Mexico 87545, USA*

[31]*Tokyo Institute of Technology, Tokyo, Japan*

[32]*Oak Ridge National Laboratory, Physics Division, Oak Ridge, Tennessee 37831, USA*

[33]*NCSR, GR-Athens, Greece*

[34]*Dipartimento di Fisica, Università di Bologna, and Sezione INFN di Bologna, I-Bologna, Italy*

[35]*Japan Atomic Energy Research Institute, Tokai-mura, Japan*

[36]*National Technical University of Athens, GR-Athens, Greece*

[37]*Institut für Isotopenforschung und Kernphysik, Universität Wien, A-Wien, Austria*

[38]*Pôle Universitaire Léonard de Vinci, F-Paris La Défense, France*

[39]*CEC-JRC-IRMM, B-Geel, Belgium*

[40]*Department of Physics–University of Basel, CH-Basel, Switzerland*
[41]*ENEA, I-Bologna, Italy*

(Received 28 November 2011; revised manuscript received 7 February 2012; published 20 April 2012)

The neutron capture cross section of ^{237}Np was measured between 0.7 and 500 eV at the CERN n_TOF facility using the 4π BaF_2 Total Absorption Calorimeter. The experimental capture yield was extracted minimizing all the systematic uncertainties and was analyzed together with the most reliable transmission data available using the SAMMY code. The result is a complete set of individual as well as average resonance parameters [$D_0 = 0.56(2)$ eV, $\langle\Gamma_\gamma\rangle = 40.9(18)$ meV, $10^4 S_0 = 0.98(6)$, $R' = 9.8(6)$ fm]. The capture cross section obtained in this work is in overall agreement with the evaluations and the data of Weston and Todd [Nucl. Sci. Eng. **79**, 184 (1981)], thus showing sizable differences with respect to previous data from Scherbakov *et al.* [J. Nucl. Sci. Technol. **42**, 135 (2005)] and large discrepancies with data Kobayashi *et al.* [J. Nucl. Sci. Technol. **39**, 111 (2002)]. The results indicate that a new evaluation combining the present capture data with reliable transmission data would allow reaching an accuracy better than 4%, in line with the uncertainty requirements of the nuclear data community for the design and operation of current and future nuclear devices.

DOI: 10.1103/PhysRevC.85.044616 PACS number(s): 25.40.Lw, 28.41.−i, 28.20.Np, 27.90.+b

I. INTRODUCTION

Neutron capture cross sections of minor actinides have gained importance in the last decade because of their key role in the design and performance of advance reactors and transmutation devices for the incineration of radioactive nuclear waste. At present, the uncertainties on such nuclear data are probably acceptable in the early phases of design feasibility studies, but in many cases the accuracies are not sufficient for the design optimization phase in which economical and safety margins are to be minimized [1–3,21].

In particular, nuclear data for ^{237}Np are of utmost importance because it is the most abundant minor actinide in the spent fuel of a commercial LWR reactor and would be responsible for the largest number of capture reactions among the minor actinides present in the core of an accelerator driven system (ADS). A detailed investigation of the results from previous capture [5–11], fission [6,12,13], and total [6,7,12–14] cross section measurements reveals significant discrepancies between experiments. Indeed, the recommended ^{237}Np evaluations do not result from the combination of several data sets as it is always desirable; instead, individual data sets are selected for each reaction channel and each neutron energy range. In particular, in the resolved resonance region the neutron and capture widths in the JENDL-4.0 evaluation are from a single transmission measurement by Gressier *et al.* [14] while the capture cross section in the unresolved resonance region is directly that from the measurement by Weston and Todd [8]. In the case of JEFF-3.1 and ENDF/B-VII.1 the resonance parameters range only up to 150 eV and are taken directly from the work of Paya [12]. Only recently, a work by Noguere [15] has combined the most recent capture and transmission data; however, high-resolution data exist only up to 100 eV, with only one data set (Weston and Todd [8]) available between 10 and 100 eV. Therefore, the results above 100 eV are based only on transmission.

The n_TOF facility provides the means for high-resolution time-of-flight measurements of capture and fission reactions, and both cross sections have been measured for the case of ^{237}Np using the Total Absorption Calorimeter (TAC) [16] and the PPAC detectors [17], respectively. This paper is devoted to the measurement and analysis of the capture data measured with the TAC, which has provided for the first time capture data with enough resolution to study resonances above the previous 100-eV limit. The details of the experiment and data reduction are given in Secs. II and III, respectively. The resonance and cross-section analysis presented in Sec. IV combines the experimental capture yield with the most reliable transmission data available at the time of this work. The results are discussed and compared to previous evaluations and experiments in Sec. V.

II. CROSS-SECTION MEASUREMENT

A. The n_TOF facility at CERN

The n_TOF (Phase-1) facility [18,19] is part of the fixed target experimental program at CERN. At n_TOF a high-intensity neutron pulse is produced every 2.4 s from spallation reactions induced by a 20-GeV/c proton beam incident on a $80 \times 80 \times 60$ cm^3 lead target. A water layer of 58 mm cools down the target and moderates the initially fast neutron energy distribution.

The result at the irradiation position (185 m) is a high instantaneous intensity neutron beam that covers the energy range from thermal to relativistic energies with a nearly isolethargic distribution between 1 eV and few tens of keV. A neutron flux of 5×10^5 neutrons/cm^2 between thermal and 10 MeV is produced by each proton pulse of the nominal intensity 7×10^{12} protons.

The precise energy dependence of the neutron fluence in the energy range of this work (1–500 eV) was determined from measurements [38] with the ^{6}Li-based silicon monitor *SiMon* that results in an evaluated shape of the neutron flux with an accuracy better than 2% in the region below a few keV. Regarding the spatial profile of the neutron beam, two collimators placed along the neutron beam line provide a nearly symmetric Gaussian-shaped profile at the sample position. In the eV region the width of this Gaussian profile is ∼5 mm, yielding a total diameter of ∼4 cm [20].

The combination of the high intensity and wide energy range of the neutron beam with *state-of-the-art* detectors and

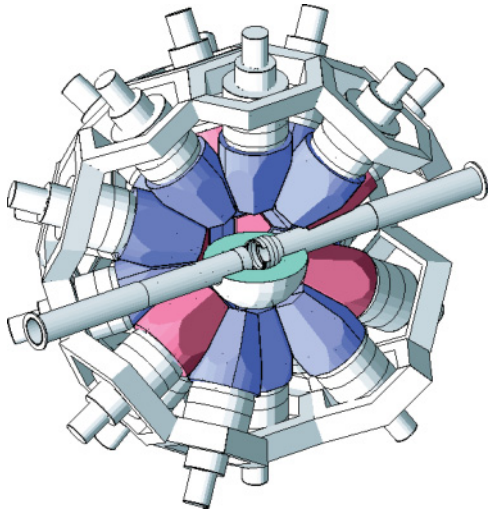

FIG. 1. (Color online) View of the Total Absorption Calorimeter as it is implemented in the code GEANT4 [33] used for the Monte Carlo simulations.

the digital data acquisition system available at n_TOF have provided in the last decade a large number of high-quality cross-section data [17,22–25] and several key contributions [26–30] regarding the measuring and analysis techniques commonly employed in *time-of-flight* experiments.

B. The Total Absorption Calorimeter

The n_TOF Total Absorption Calorimeter (TAC) is a 4π segmented array made of 40 BaF_2 crystals with pentagonal and hexagonal shapes specifically built for detecting the Γ-ray cascades emitted in neutron capture reactions. Full details on the characteristics and performance of the detector are given in Ref. [16].

The 40 crystals are encapsulated in ^{10}B-loaded carbon fiber and form a spherical shell of 15-cm thickness, with an inner diameter of 21 cm (see Fig. 1). The TAC shows a nearly 100% efficiency for detecting capture cascades with energy resolutions of 16% at 662 keV and 6% at 6.1 MeV. A 5-cm-thick spherical shell made of $^{6}Li_2C_{12}H_{20}O_4$ is placed in the inner hole of the TAC for moderating and partially absorbing the neutrons that are scattered in the sample. The combination of this moderator with the ^{10}B-loaded carbon fiber capsules results in a neutron sensitivity (i.e., efficiency for detecting neutrons) lower than 1% in the neutron energy range of interest.

The combined characteristics of the TAC and the n_TOF facility provide the means for performing high-quality neutron capture measurements of small mass and/or radioactive samples. For instance, (a) the high efficiency of the TAC and the high intensity of the n_TOF neutron flux allow reducing the background caused by the intrinsic activity in the case of radioactive samples, and (b) the high total absorption efficiency, segmentation, and good energy resolution of the detector allow discriminating between different reactions on the basis of their Q values and Γ-ray multiplicities. The latter is a powerful tool for improving the capture over background ratio, as illustrated in Sec. III A.

C. Data acquisition and event reconstruction

The BaF_2 crystals are coupled to 5″ Photonis XP4508B photomultipliers and special voltage dividers made at the Instituto Tecnológico e Nuclear in Lisbon that favor a fast recovery of the photomultipliers. In the standard configuration of the n_TOF data acquisition system [29] the anode signals are recorded by 40 channels of high-performance digitizers (Acqiris-DC270) with 8 bits resolution and 8-MB memory operated at 500 MSamples/s. This system records for each accelerator pulse 16-ms-long data buffers which contain the digitized electronic response of each BaF_2 module for neutron energies above 0.7 eV.

The data buffers are analyzed offline by a dedicated pulse shape reconstruction algorithm [35]: For each recorded signal the routine returns the associated time-of-flight (TOF), the amplitude and integrals corresponding to the fast and slow scintillation components, the particle type (Γ-ray or α), and the corresponding BaF_2 module number. The energy calibration of each module is obtained from the amplitude distribution of the slow component measured for standard calibration sources (^{137}Cs, ^{60}Co, ^{88}Y, ^{24}Na, and Pu/C) and the possible gain drifts are monitored continuously by looking at the position in the amplitude spectrum of the α signals produced by the decay of Ra impurities in the crystals. The individual energy calibrated signals are finally grouped, using a coincidence window of 20 ns, into TAC events characterized by their TOF (and the associated neutron energy E_n), deposited energy $E_{\rm sum}$ and crystal multiplicity $m_{\rm cr}$ (number of BaF_2 modules firing).

D. The ^{237}Np and auxiliary samples

A 49.1-mg NpO_2 sample of 10-mm diameter was prepared at the Institute for Physics and Power Engineering at Obnisk (Russia) [34] with a purity of 99.2%, with ^{238}Pu as the only contaminant. The oxide powder was deposited on a 72-mg aluminium backing and then encapsulated between two titanium layers weighting 420 mg. The sample assembly, with an activity of 1.29 MBq, was sealed and certified ISO-2919 as requested by the safety authorities at CERN.

Additionally, a set of samples was prepared for identifying and quantifying the different background contributions: a graphite sample for the characterization of the TAC response to scattered neutrons, a ^{197}Au sample for normalization purposes and validation of the analysis tools, and a dummy sample (empty Ti-Al canning) to determine the contribution of the sample's assembly.

The main characteristics of the neptunium and auxiliary samples are listed in Table I.

III. DATA REDUCTION

The data reduction consists in the determination of the experimental capture yield (i.e., reaction rate) from the measured distributions of E_n, $E_{\rm sum}$, and $m_{\rm cr}$. The same procedure was applied for all samples listed in Table I. The capture yield is defined as the number of incident neutrons undergoing

TABLE I. Main characteristics of the neptunium and auxiliary samples.

Sample	Diameter (mm)	Mass (mg)	Thickness (atoms/barn)	Neutron pulses ($\times 10^3$)
^{237}Np	10	43.3(13)	$1.40(4)\times10^{-4}$	54
^{197}Au	10	185.4(1)	$7.22(4)\times10^{-4}$	89
Graphite	10	70.0(1)	$4.47(6)\times10^{-3}$	23
Dummy	–	–	–	21

a capture reaction in the ^{237}Np sample and is calculated experimentally as

$$Y_{n,\gamma}(E_n) = \frac{C_{\rm tot}(E_n) - C_{\rm bck}(E_n)}{\varepsilon \cdot F_{\rm BIF} \cdot \phi_n(E_n)}, \qquad (1)$$

where $C_{\rm tot}(E_n)$ and $C_{\rm bck}(E_n)$ are the total and background counts, ε is the detection efficiency of the TAC, $\phi_n(E_n)$ is the neutron fluence as given by the *SiMon* monitor, and $F_{\rm BIF}$ is the beam interception factor. The latter takes into account that the samples (1-cm diameter) are smaller than the beam (4-cm diameter) and thus only a fraction of the monitored $\phi_n(E_n)$ is impinging on the sample. Each of the components of Eq. (1) is discussed in detail in the following subsections.

A. Background and selection of analysis conditions

The various components contributing to the overall background in the capture measurement have been determined from dedicated measurement of the auxiliary samples (see Ref. [16] for details). The response of the TAC to these samples, including the neptunium one, is displayed in Fig. 2. All distributions are normalized to the incident beam intensity in the form of nominal proton pulses (see Sec. II A). The detector response to capture cascades from ^{237}Np is observed as a peak at 5 MeV, corresponding to total absorption of the capture cascade, and the associated tail at lower energies. The other structures correspond to background from the different reactions, as labeled in the figure: The major components of the background are from the activity of the ^{237}Np sample (observed only at low energies), the activity from β decays occurring in the BaF_2 crystals (with Q values as large as 5 MeV from the ^{208}Tl β decay), and the neutron capture and scattering reactions taking place in the Ti of the sample's assembly and the Ba forming the crystals.

The characteristics of the TAC (segmentation, high detection, and total absorption efficiency and good energy resolution) allow optimizing the capture to background ratio by selecting an appropriate set of conditions in $m_{\rm cr}$ and $E_{\rm sum}$. For instance, Fig. 3 shows the energy deposition in the TAC in the ^{237}Np measurement for different conditions in crystal multiplicity in the neutron energy range from 1 to 10 eV, where many capture resonances are present. It is seen that the impact of different background components is reduced when more restrictive conditions on the crystal multiplicity are imposed. For instance, the contribution from the activity of the sample (1.29 MBq) is eliminated completely when applying a condition such as $m_{\rm cr} > 1$ and $E_{\rm sum} > 500$ keV. A detailed analysis of the capture to background ratio under different conditions has lead to the optimum values adopted for the analysis: $m_{\rm cr} > 2$ and $2.5 < E_{\rm sum}({\rm MeV}) < 6$. The corresponding neutron energy distributions are shown in Fig. 4, where the ^{237}Np resonances are well above the background even beyond the 500-eV limit of the resolved resonance region. As expected, the contribution of the background is smooth except for the small structures observed around 30 and 100 eV corresponding to resonances in the Ba(n,γ) cross section.

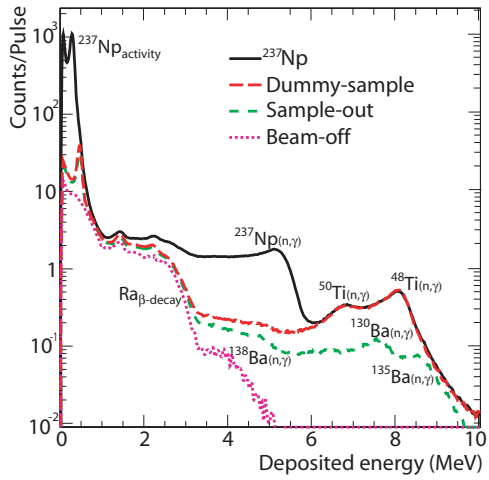

FIG. 2. (Color online) Deposited energy distribution measured with the neptunium and the auxiliary samples. The data correspond to neutron energies between 1 and 10 eV.

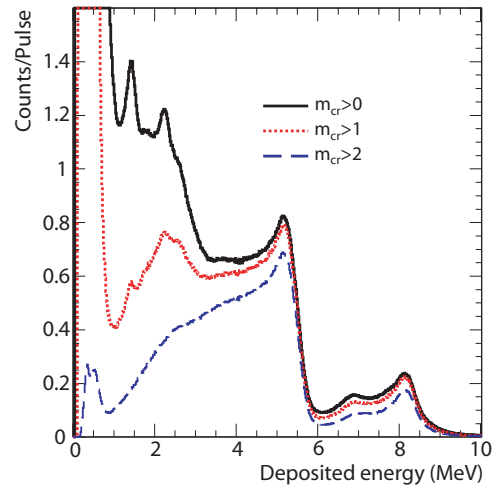

FIG. 3. (Color online) Deposited energy distribution from ^{237}Np(n,γ) under different conditions in multiplicity. The data correspond to neutron energies between 1 and 10 eV.

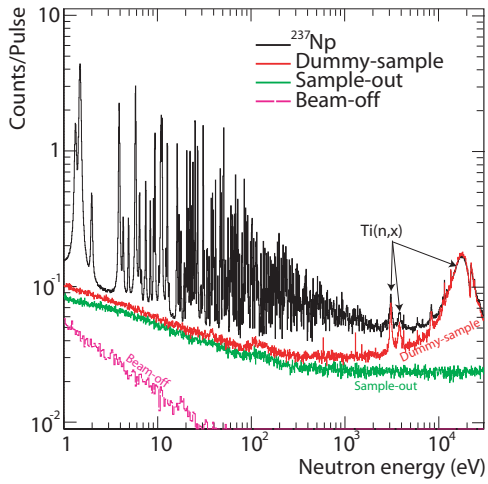

FIG. 4. (Color online) Neutron energy distribution measured with the neptunium and auxiliary samples under the conditions $m_{cr} > 2$ and $2.5 < E_{sum}(\text{MeV}) < 6$.

The background associated with neutron scattering in the ^{237}Np sample itself is very difficult to estimate and to subtract. In this case, however, such a background is negligible in most of the neutron energy range because the capture cross section is approximately three orders of magnitude larger than the elastic cross section, and the efficiency for detecting capture events is two orders of magnitude larger than the neutron sensitivity [16]. The contribution of such background is maximum in the interval between resonances above 400 eV, and even in that region it contributes less than 5% to the measured yield in between resonances.

B. Detection efficiency

The large solid angle coverage of the TAC and the 15-cm thickness of the crystals provide a nearly 100% detection efficiency (ε) for capture cascades. However, this value decreases when analysis conditions in E_{sum} and m_{cr} are applied. In such a case, Monte Carlo simulations are best suited for determining the detection efficiency of the TAC that becomes dependent on the selected analysis conditions TAC $\varepsilon(E_{sum}, m_{cr})$ [32].

The GEANT4 [33] simulation package was used for this purpose. The detector geometry was implemented in detail including the BaF_2 crystals, their carbon fiber capsules, the neutron absorber, the photomultipliers, and the structural materials. The geometry (see Fig. 1) and physics of the simulation have been validated against data from monoenergetic γ-ray sources and neutron capture reactions with a known decay pattern. The DECAYGEN code [36] was used for the generation of capture cascades and the parameters of the photon strength function taken from RIPL-2 [48] were adjusted to reproduce the experimental data under any condition on E_{sum} and m_{cr}. Full details on the simulation and the generation of capture cascades are given in [32] and [37] for the particular case of actinides.

An innovative method [30] was developed for calculating the effect of pile-up and dead-time losses. These have been shown to be sizable only for counting rates beyond 0.5 counts/μs and thus are negligible in this measurement even at the top of the strongest resonances where the recorded counting rate is always below 0.4 counts/μs.

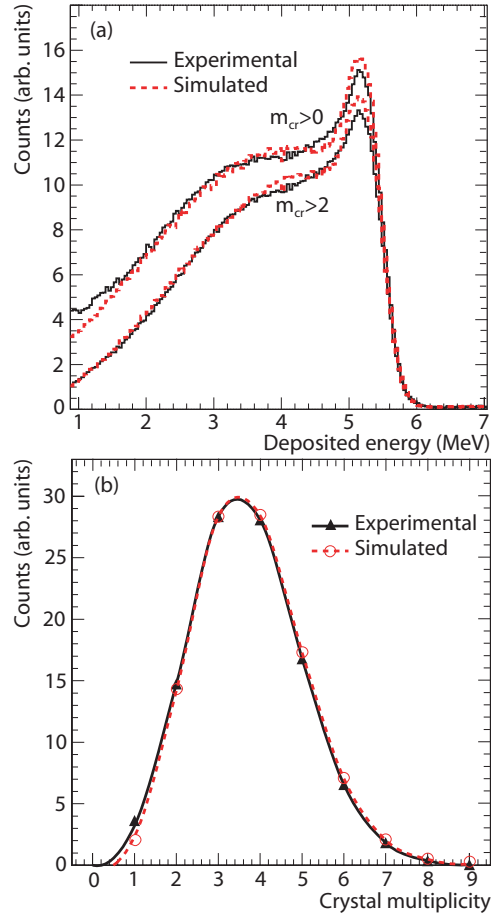

FIG. 5. (Color online) Measured and simulated TAC response corresponding to the ^{237}Np ($E_n = 1.32$ eV, $J = 3^+$). (a) Deposited energy distribution with and without conditions in m_{cr}. (b) crystal multiplicity distribution ($E_{sum} > 1$ MeV).

Once all the effects are taken into account, an accurate determination of the detection efficiency can be obtained from Monte Carlo simulations. Figure 5 illustrates the excellent agreement between simulated and experimental data in the form of deposited energy (a) and crystal multiplicity (b). The results from the simulation provide a value for the detection efficiency $\varepsilon(m_{cr} > 2, E_{sum} > 2.5$ MeV) of 0.70(2). Because of the high detection efficiency of the TAC and the large level density of ^{238}Np, it was found experimentally that the efficiency value remains the same for all resonances independently of their spin.

C. Incident neutron fluence and beam interception factor

Because of the use of a neptunium sample smaller than the beam, only part of the neutron beam is impinging on the samples. The calculation of the fraction F_{BIF} of the beam incident on the sample (beam interception factor) is accomplished by means of the saturated resonance method (SRM) [39], measuring a thick gold sample of the same

diameter as the neptunium one and placed at exactly the same position, thus seeing a similar fraction of the neutron beam. In the SRM method, the thickness of the sample and the gold cross section at the 4.9-eV resonance are such that all (with some corrections) incident neutrons are captured and therefore the number of capture reactions occurring at the flat top of the resonance provides directly the total number of incident neutrons at that energy. A beam interception factor of 19.1% was found, in agreement with the expected value from the information available on the beam spatial profile.

D. Normalization associated with the uncertainty in the sample mass

The ^{237}Np sample was provided by the IPPE (Obnisk-Russia) [34] within a package containing also other actinide samples such as ^{233,234}U, ^{240}Pu, and ^{243}Am. A systematic characterization of all of them has provided evidence that the mass and impurities reported by the manufacturer are not always accurate. Therefore, although the results from the characterization of ^{237}Np did not reveal the presence of contaminants, the total mass of neptunium may be affected by an uncertainty larger than the 3% value claimed by the manufacturer.

The strategy that was followed in this work for the analysis of the ^{237}Np cross section is to perform a combined analysis of the capture data and the most reliable transmission data available (Gressier *et al.* [14]), which are also used for normalization. This strategy not only prevents any normalization problem associated with the uncertainty in the mass of the sample but also provides a more accurate determination of the resonance parameters because it is using two independent data sets (of different reactions) to determine the two reaction widths.

The results and conclusions that follow correspond to such an analysis strategy. However, the resonance analysis was carried out as well without the normalization to transmission, leading both analysis methods to results in agreement within 6%. Such a difference can be explained as a combination of the uncertainty in the mass of neptunium and the additional systematic uncertainty in the data reduction process, dominated by the calculation of ε and F_{BIF} (see Table II).

TABLE II. Summary of the relative (%) systematic uncertainties associated with the measurement and the calculation of the capture yield.

	Not normalized to transmission	Normalized to transmission
	RRR	RRR
Sample mass	3[a]	–
Detection efficiency	2.8	–
Incident neutron flux	2.6	–
Shape of neutron flux	2	2
Background	1	1
Transmission data	–	3
Total ($\sqrt{\Sigma x_i^2}$)	5.3	3.7

[a]As declared by the manufacturer.

E. Discussion on uncertainties

The different contributions to the overall uncertainty of the experimental capture yield are summarized in Table II and discussed one by one in the following:

(i) *Sample mass*. As mentioned in the previous section, the uncertainty in the mass of neptunium provided by the manufacturer is 3%.

(ii) *Detection efficiency*. As mentioned in Sec. III B (see [32] for more details), the uncertainty in the detection efficiency computed by the Monte Carlo method is dominated by the unknown electromagnetic de-excitation scheme of the compound nucleus. A statistical model relying on a parametrized level density and photon strength functions for $E1$, $E2$, and $M1$ transitions for computing the branching ratios is used, and the values of the efficiency do depend on the initial assumptions made. The associated uncertainty was estimated as the standard deviation of the efficiencies obtained in a large number of simulations with different PSF yielding results in agreement with the experimental data.

(iii) *Incident neutron fluence*. The overall uncertainty in the determination of the number of incident neutrons is given by the stability of the neutron monitoring with *SiMon* (1% stability along the entire measurement), the uncertainty in the determination of the saturation level for the gold resonance at 4.9 eV (dominated by the uncertainty in the detection efficiency of ^{197}Au, which is 2.2%), and any possible variation in the positioning of the gold and neptunium samples that would lead to a change in F_{BIF} (<1%). The squared sum of such uncertainties leads to an overall uncertainty of the incident neutron fluence at 4.9 eV of 2.6%.

(iv) *Neutron energy shape of the flux*. The uncertainty in the energy dependence of the neutron flux in the range of interest (below 1 keV) is 2% [23], and it is associated mainly with the uncertainty in the reference cross section ^{6}Li(n,α).

(v) *Background*. The smooth background level is sizable only between resonances and is well determined by dedicated measurements. The uncertainty associated with the background corrections of the yield is less than 1% for most resonances.

(vi) *Transmission data*. The uncertainty in the transmission measurement data of Gressier *et al.* [14] is 3% according to the authors.

The normalization of the capture yield to the transmission data replaces all the uncertainties related to scaling factors (mass, detection efficiency, and incident neutron fluence) by the uncertainty of the transmission data. The comparison of the two methods (i.e., with and without normalization to transmission) is summarized in Table II.

The total uncertainties listed in Table II correspond to the root of the squared sum of the partial uncertainties. It is seen that the total uncertainty is significantly reduced when the capture yield is normalized to the transmission. The combined analysis of capture and transmission data results in a capture

cross section with an accuracy better than 4%, while the analysis of capture data alone is affected by an uncertainty of around 5%.

IV. CROSS-SECTION ANALYSIS

The resolved resonance region (RRR) of ^{237}Np extends up to 150 eV in the JEFF-3.1 and ENDF/B-VII.1 evaluations, and up to 500 eV in the JENDL-4.0 evaluation, which is based on transmission [14] and fission [13] measurements only. Indeed, the present capture cross-section measurement is unique in the sense that its unprecedented resolving power (from the 185-m flight path) and excellent statistics allow analyzing capture resonances in the entire resonance region for the first time.

A. Resonance analysis strategy with SAMMY

In the resonance region, the capture yield and transmission data are described by means of the R-matrix formalism in terms of individual resonance parameters:

$$RP_i = (R', E_i, J_i^{\pi}, \ell_i, \Gamma_{\gamma i}, \Gamma_{ni}, \Gamma_{fi}), \quad (2)$$

where R' is the R-matrix scattering radius of the nucleus; E_i, J_i^{π}, ℓ_i are the energy, spin parity, and orbital momentum of each resonance; and the widths $\Gamma_{\gamma i}$, Γ_{ni}, and Γ_{fi} are related to the capture, scattering, and fission probabilities in each resonance, respectively.

In this work, the resonance parameters E_i, $\Gamma_{\gamma i}$, and Γ_{ni} have been determined with the R-matrix code SAMMY (Version 7.0.0) [41], which uses a sequential Bayesian method for providing the set of resonance parameters that fits better the experimental capture and transmission data from this work and Gressier *et al.* [14], respectively. The SAMMY code includes in the fitting process all the experimental corrections associated with the sample (mainly self-shielding, multiple scattering, and Doppler broadening) and the facility (i.e., the time-of-flight to neutron energy distribution) referred to as resolution function [42].

Some comments regarding the resonance analysis follow:

(i) The Reich-Moore formalism option was chosen in SAMMY.

(ii) All resonances have been considered to be s wave ($\ell_i = 0$).

(iii) The results are not affected by the detailed knowledge of the resolution function because at these energies the broadening is dominated by the Doppler effect, which was modeled using the free gas model with a temperature of 27° C.

(iv) The spin and parity of all resonances have been taken from JENDL-4.0.

(v) Following the trend from recent investigations [43,44] a thermal cross section of 181 barns was considered instead of the value of 161 barns found in the present evaluations. The negative resonance parameters describing the 1/v region have been chosen accordingly: $E_{\rm res} = -1$ eV, $\Gamma_\gamma = 40.5$ meV, $\Gamma_n = 2.27$ meV, $\Gamma_f = 0.441\ \mu$eV.

(vi) The scattering radius R' was determined from the analysis of transmission data in the region between resonances from 12 to 35 eV, resulting in the values $R'_{J=2} = 10.7(2)$ fm and $R'_{J=3} = 9.8(2)$ fm, thus $R' = 10.2(4)$ fm.

(vii) In a first iteration, the radiative widths $\Gamma_{\gamma i}$ have been determined individually in the low-energy region where the resonances are well resolved. Then, the weighted mean computed from the lower energy resonances was adopted and kept fixed along the fitting process for all the resonances (more details are given in the next section).

(viii) Transmission and capture data have been analyzed sequentially, using as input the output from the previous fit until convergence was reached. The details of this methodology are given in the SAMMY manual [41] and have been applied in previous evaluations [40].

(ix) A normalization factor scaling the capture yield and a constant background have been fitted in each of the intervals in which the resonance region was divided. The resulting values are discussed in Sec. IV D

B. Results below 43 eV

The result of the fits of the capture yield and transmission data are shown in Figs. 6 and 7, where the points correspond to the experimental data and the black lines to the results of the SAMMY fits. The figures illustrate the excellent resolving power of the capture and transmission data and the quality of the fit, which has provided a set of resonance parameters compatible with both data sets.

The set of parameters for all the resonances below 43 eV is listed in Table III, while the full set of parameters of the 657 resonance below 500 eV is available in the EXFOR database [53]. The table includes as well the resonance parameters from the JENDL-4.0 evaluation and those from the recent work of Noguere. However, the discussion of our results and the comparison with previous works is addressed better in terms of average cross sections and average resonance parameters (see Sec. V).

Regarding the resonance widths given in Table III, as mentioned before, they are expected to remain essentially constant, at most with small fluctuations around the average value (see [45]). Thus, in a first iteration we have calculated the average radiative width $\langle\Gamma_\gamma\rangle$ below 43 eV and have kept it fixed for all resonances in the final fits. The calculated value of $\langle\Gamma_\gamma\rangle$ is 40.9(18) meV, where the uncertainty corresponds to the variation around the mean value when $\langle\Gamma_\gamma\rangle$ is calculated in different energy ranges within the 1–43 eV range. Such uncertainty (4.4%) is reasonable considering that a detailed investigation by Gressier *et al.* [47] and Courcelle *et al.* [46] showed that the associated error in the determination of the individual and average values of the radiative width at low energies (from the use of the free gas model for modeling the Doppler broadening instead of a more accurate harmonic crystal lattice model) can be as large as 7% and 3.4%, respectively.

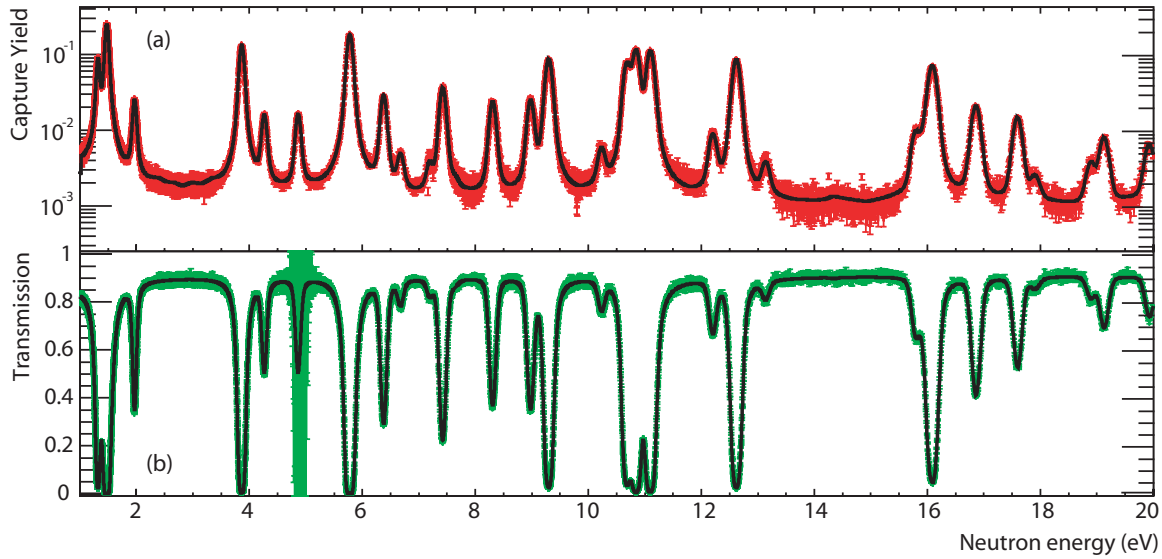

FIG. 6. (Color online) SAMMY fits (solid lines) to the capture yield (red markers) and the transmission (green markers) data between 1 and 20 eV.

The energy and the neutron width of all the resonances have been fitted and the results are given in Table III. Regarding the associated uncertainties, in the case of the energy there is a source of uncertainty intrinsic to the facility which is its energy resolution. This was properly quantified by Coceva *et al.* [42] and ranges between 5×10^{-4} at 1 eV and 10^{-3} around 500 eV. Thus, the table contains the energy uncertainty given by SAMMY except in those cases when it is smaller than the energy resolution of n_TOF, in which case the latter is given. In the case of the neutron widths, the high quality of fit to the capture and transmission data sets and the reduction of the uncertainties along the sequential fitting process are such that the uncertainties given by SAMMY are very small, even lower than 0.1% for the neutron width in some cases. However, when one considers that the area of the resonances is directly proportional to Γ_n and nearly independent of Γ_γ because $\Gamma_\gamma \gg \Gamma_n$, it becomes clear that the minimum uncertainty of the neutron width is that of the capture yield: 3.7% (see Table II). Thus, as a conservative approach, when the uncertainty in Γ_n given by SAMMY is smaller than 3.7%, the latter value is considered instead.

The short- and long-range correlations between resonance parameters, considering as well the normalization and background values, have been studied in the first iteration, where the radiative widths are also fitted with SAMMY. Figure 8 shows the correlation matrix betwen the 107 parameters in the energy range between 1 and 43 eV: three for each resonance (No. 1 to No. 105) and the last two corresponding to the

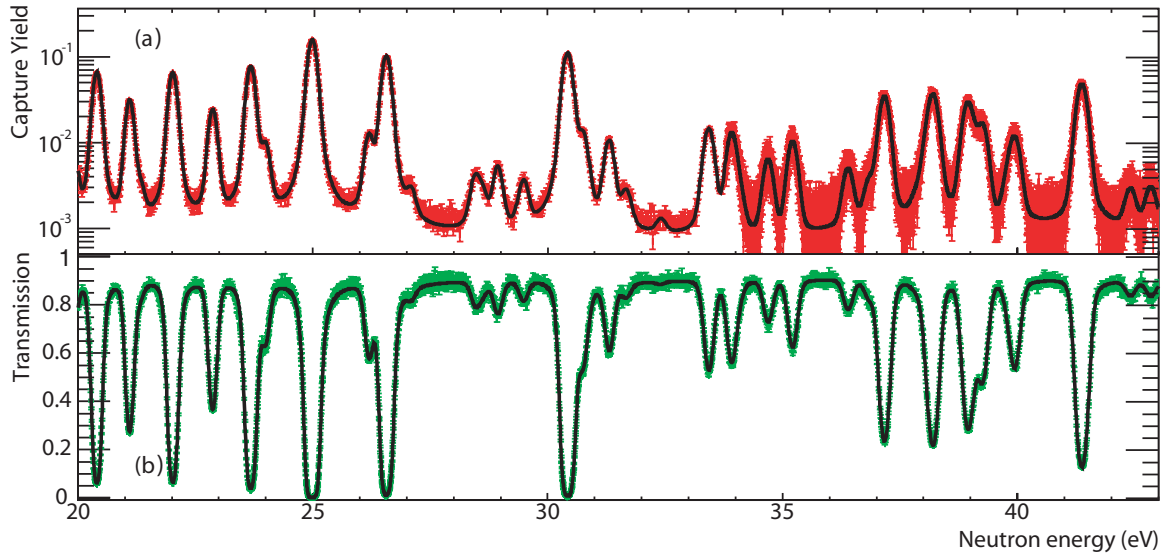

FIG. 7. (Color online) SAMMY fits (solid lines) to the capture yield (red markers) and the transmission (green markers) data between 20 and 43 eV.

TABLE III. Resonance parameters between 1 and 43 eV (73 resonances) from this work, the recommended evaluation JENDL-4.0, and the work by Noguere. The resonance spins are taken from JENDL-4.0. The resonance parameter uncertainties reported in this work are those given by SAMMY. These result from the propagation of the uncertainties and the correlation between resonance parameters through the sequential fit of the capture and transmission data (see Ref. [40]).

Energy	J^π	This work		JENDL-4.0		Noguere	
(eV)		Γ_γ(meV)	Γ_n(meV)	Γ_γ(meV)	Γ_n(meV)	Γ_γ(meV)	Γ_n(meV)
1.321 ± 0.001	3	40.9 ± 1.8	0.0317 ± 0.0012	40.3	0.0320	37.9 ± 0.4	0.0310 ± 0.0010
1.478 ± 0.001	2	40.9 ± 1.8	0.181 ± 0.007	40.5	0.1840	41.6 ± 0.9	0.1840 ± 0.0040
1.969 ± 0.001	3	40.9 ± 1.8	0.0140 ± 0.0005	39.5	0.0140	37.2 ± 0.6	0.0140 ± 0.0010
3.865 ± 0.002	3	40.9 ± 1.8	0.207 ± 0.008	39.7	0.2120	40.4 ± 0.6	0.2110 ± 0.0020
4.264 ± 0.003	2	40.9 ± 1.8	0.0323 ± 0.0012	40.4	0.0330	40.0 ± 0.9	0.0330 ± 0.0010
4.863 ± 0.003	2	40.9 ± 1.8	0.0396 ± 0.0015	40.0	0.0420	40.1 ± 1.2	0.0430 ± 0.0010
5.777 ± 0.004	3	40.9 ± 1.8	0.524 ± 0.019	41.9	0.5280	42.1 ± 0.8	0.5330 ± 0.0090
6.378 ± 0.004	3	40.9 ± 1.8	0.0779 ± 0.0029	39.6	0.0790	38.8 ± 1.2	0.0790 ± 0.0010
6.677 ± 0.004	2	40.9 ± 1.8	0.0136 ± 0.0005	40.1	0.0130	39.3 ± 1.0	0.0140 ± 0.0010
7.189 ± 0.005	2	40.9 ± 1.8	0.00823 ± 0.00030	40.0	0.0090	39.3 ± 1.0	0.0100 ± 0.0010
7.423 ± 0.005	3	40.9 ± 1.8	0.119 ± 0.004	38.4	0.1220	39.0 ± 1.5	0.1240 ± 0.0010
7.678 ± 0.007	2	40.9 ± 1.8	0.00176 ± 0.00012	40.0	0.0020	39.3 ± 1.0	0.0030 ± 0.0010
8.307 ± 0.006	3	40.9 ± 1.8	0.0879 ± 0.0033	37.6	0.0900	39.7 ± 1.4	0.0930 ± 0.0010
8.978 ± 0.006	3	40.9 ± 1.8	0.101 ± 0.004	37.0	0.1020	37.2 ± 1.3	0.1040 ± 0.0010
9.299 ± 0.006	2	40.9 ± 1.8	0.585 ± 0.022	41.4	0.6020	41.8 ± 0.9	0.6110 ± 0.0060
10.231 ± 0.007	2	40.9 ± 1.8	0.0275 ± 0.0010	40.0	0.0280	39.3 ± 1.0	0.0300 ± 0.0010
10.682 ± 0.007	3	40.9 ± 1.8	0.422 ± 0.016	40.0	0.4320	39.3 ± 1.0	0.4390 ± 0.0050
10.845 ± 0.008	3	40.9 ± 1.8	0.683 ± 0.025	40.0	0.6890	39.3 ± 1.0	0.7010 ± 0.0110
11.097 ± 0.008	2	40.9 ± 1.8	0.996 ± 0.037	43.8	1.0100	42.2 ± 1.1	1.0320 ± 0.0130
12.202 ± 0.009	3	40.9 ± 1.8	0.0487 ± 0.0018	40.0	0.0490	39.3 ± 1.0	0.0480 ± 0.0010
12.618 ± 0.009	2	40.9 ± 1.8	0.888 ± 0.033	40.2	0.9110	38.9 ± 1.2	0.9250 ± 0.0100
13.139 ± 0.009	3	40.9 ± 1.8	0.0178 ± 0.0007	40.0	0.0170	39.3 ± 1.0	0.0170 ± 0.0010
14.282 ± 0.031	2	40.9 ± 1.8	0.000962 ± 0.000099	40.0	0.0020	39.3 ± 1.0	0.0020 ± 0.0010
15.796 ± 0.012	3	40.9 ± 1.8	0.0671 ± 0.0025	40.0	0.0690	39.3 ± 1.0	0.0690 ± 0.0010
15.949 ± 0.012	3	40.9 ± 1.8	0.0374 ± 0.0018	40.0	0.0380	39.3 ± 1.0	0.0380 ± 0.0010
16.089 ± 0.012	2	40.9 ± 1.8	1.01 ± 0.04	40.0	1.0520	38.1 ± 1.8	1.0690 ± 0.0120
16.860 ± 0.012	2	40.9 ± 1.8	0.290 ± 0.011	37.8	0.2990	39.3 ± 1.0	0.3040 ± 0.0020
17.597 ± 0.013	3	40.9 ± 1.8	0.151 ± 0.006	39.1	0.1560	39.3 ± 1.0	0.1590 ± 0.0010
17.908 ± 0.013	2	40.9 ± 1.8	0.0155 ± 0.0007	40.0	0.0180	39.3 ± 1.0	0.0180 ± 0.0010
17.935 ± 0.039	3	40.9 ± 1.8	0.00299 ± 0.00029	40.0	0.0030	39.3 ± 1.0	0.0030 ± 0.0010
18.892 ± 0.014	2	40.9 ± 1.8	0.0418 ± 0.0015	40.0	0.0480	39.3 ± 1.0	0.0480 ± 0.0010
19.126 ± 0.014	3	40.9 ± 1.8	0.0838 ± 0.0031	40.0	0.0880	39.3 ± 1.0	0.0890 ± 0.0010
19.932 ± 0.015	3	40.9 ± 1.8	0.0622 ± 0.0023	40.0	0.0700	39.3 ± 1.0	0.0690 ± 0.0010
20.403 ± 0.015	2	40.9 ± 1.8	1.30 ± 0.05	39.4	1.3680	37.1 ± 1.9	1.3950 ± 0.0150
21.103 ± 0.016	3	40.9 ± 1.8	0.429 ± 0.016	40.0	0.4460	39.3 ± 1.0	0.4500 ± 0.0030
21.345 ± 0.016	2	40.9 ± 1.8	0.0254 ± 0.0011	40.0	0.0280	39.3 ± 1.0	0.0320 ± 0.0010
22.021 ± 0.017	2	40.9 ± 1.8	1.46 ± 0.05	39.5	1.4980	36.5 ± 1.8	1.5210 ± 0.0180
22.871 ± 0.017	3	40.9 ± 1.8	0.375 ± 0.014	38.5	0.3800	38.2 ± 2.4	0.3860 ± 0.0030
23.681 ± 0.018	3	40.9 ± 1.8	1.39 ± 0.05	38.0	1.4200	39.3 ± 1.0	1.4360 ± 0.0180
23.991 ± 0.018	2	40.9 ± 1.8	0.179 ± 0.007	40.0	0.1910	39.3 ± 1.0	0.1820 ± 0.0020
24.757 ± 0.019	3	40.9 ± 1.8	0.0503 ± 0.0022	40.0	0.0260	39.3 ± 1.0	0.0340 ± 0.0060
24.989 ± 0.019	3	40.9 ± 1.8	3.56 ± 0.13	40.0	3.6650	39.3 ± 1.0	3.6610 ± 0.0590
26.200 ± 0.020	3	40.9 ± 1.8	0.211 ± 0.008	40.0	0.1990	39.3 ± 1.0	0.1960 ± 0.0020
26.567 ± 0.021	3	40.9 ± 1.8	2.31 ± 0.09	40.7	2.3360	39.3 ± 1.0	2.3890 ± 0.0390
27.086 ± 0.021	2	40.9 ± 1.8	0.0433 ± 0.0016	40.0	0.0380	39.3 ± 1.0	0.0390 ± 0.0010
28.448 ± 0.022	2	40.9 ± 1.8	0.0926 ± 0.0034	40.0	0.0940	39.3 ± 1.0	0.0930 ± 0.0060
28.618 ± 0.022	3	40.9 ± 1.8	0.0359 ± 0.0018	40.0	0.0310	39.3 ± 1.0	0.0310 ± 0.0070
28.938 ± 0.023	2	40.9 ± 1.8	0.140 ± 0.005	40.0	0.1370	39.3 ± 1.0	0.1380 ± 0.0020
29.484 ± 0.023	2	40.9 ± 1.8	0.0847 ± 0.0031	40.0	0.0840	39.3 ± 1.0	0.0830 ± 0.0020
30.424 ± 0.024	3	40.9 ± 1.8	3.10 ± 0.11	38.2	3.1450	39.3 ± 1.0	3.1350 ± 0.0550
30.756 ± 0.024	2	40.9 ± 1.8	0.344 ± 0.013	40.0	0.3710	39.3 ± 1.0	0.3580 ± 0.0070
31.311 ± 0.025	3	40.9 ± 1.8	0.243 ± 0.009	40.0	0.2450	39.3 ± 1.0	0.2450 ± 0.0030
31.673 ± 0.025	3	40.9 ± 1.8	0.0452 ± 0.0017	40.0	0.0430	39.3 ± 1.0	0.0420 ± 0.0010

TABLE III. (*Continued.*)

Energy	J^π	This work		JENDL-4.0		Noguere	
(eV)		Γ_γ(meV)	Γ_n(meV)	Γ_γ(meV)	Γ_n(meV)	Γ_γ(meV)	Γ_n(meV)
32.476 ± 0.026	2	40.9 ± 1.8	0.0131 ± 0.0009	40.0	0.0110	39.3 ± 1.0	0.0110 ± 0.0020
33.430 ± 0.027	3	40.9 ± 1.8	0.387 ± 0.014	40.0	0.3950	39.3 ± 1.0	0.3950 ± 0.0050
33.913 ± 0.027	2	40.9 ± 1.8	0.437 ± 0.016	40.0	0.4870	39.3 ± 1.0	0.4870 ± 0.0060
34.056 ± 0.027	3	40.9 ± 1.8	0.0376 ± 0.0033	40.0	0.0350	39.3 ± 1.0	0.0390 ± 0.0060
34.688 ± 0.028	3	40.9 ± 1.8	0.145 ± 0.005	40.0	0.1700	39.3 ± 1.0	0.1630 ± 0.0020
35.210 ± 0.028	2	40.9 ± 1.8	0.367 ± 0.014	40.0	0.4090	39.3 ± 1.0	0.4130 ± 0.0040
36.391 ± 0.029	3	40.9 ± 1.8	0.112 ± 0.004	40.0	0.1260	39.3 ± 1.0	0.1210 ± 0.0020
36.850 ± 0.030	2	40.9 ± 1.8	0.0843 ± 0.0031	40.0	0.0870	39.3 ± 1.0	0.0850 ± 0.0030
37.163 ± 0.030	3	40.9 ± 1.8	1.07 ± 0.04	37.4	1.1380	39.3 ± 1.0	1.1520 ± 0.0110
37.902 ± 0.031	2	40.9 ± 1.8	0.0397 ± 0.0040	40.0	0.0420	39.3 ± 1.0	0.0420 ± 0.0040
38.074 ± 0.031	2	40.9 ± 1.8	0.233 ± 0.019	40.0	0.2080	39.3 ± 1.0	0.2080 ± 0.0070
38.203 ± 0.031	3	40.9 ± 1.8	1.10 ± 0.04	40.0	1.1930	39.3 ± 1.0	1.1990 ± 0.0130
38.923 ± 0.031	3	40.9 ± 1.8	0.726 ± 0.030	40.0	0.8160	39.3 ± 1.0	0.8200 ± 0.0130
39.006 ± 0.032	2	40.9 ± 1.8	0.411 ± 0.037	40.0	0.4100	39.3 ± 1.0	0.4100 ± 0.0140
39.244 ± 0.032	3	40.9 ± 1.8	0.514 ± 0.019	40.0	0.5290	39.3 ± 1.0	0.5320 ± 0.0070
39.837 ± 0.032	2	40.9 ± 1.8	0.0906 ± 0.0087	40.0	0.0880	39.3 ± 1.0	0.0880 ± 0.0040
39.937 ± 0.032	3	40.9 ± 1.8	0.418 ± 0.015	40.0	0.4500	39.3 ± 1.0	0.4530 ± 0.0050
41.366 ± 0.034	3	40.9 ± 1.8	1.82 ± 0.07	38.9	1.9470	39.3 ± 1.0	1.9630 ± 0.0270
42.412 ± 0.035	3	40.9 ± 1.8	0.0590 ± 0.0022	40.0	0.0840	39.3 ± 1.0	0.0840 ± 0.0170
42.837 ± 0.035	3	40.9 ± 1.8	0.0732 ± 0.0027	40.0	0.0830	39.3 ± 1.0	0.0830 ± 0.0040

normalization (No. 106) and constant background (No. 107) variables, respectively. The red lines in the figure indicate a distance of nine resonance parameters, which corresponds to three consecutive resonances. It is observed that there are clear correlations between neighboring resonances within the mentioned three resonances' distance limit, especially between those that are observed as clusters in Fig. 4. Longer range correlations exist only for the strongest resonances, which are the lowest lying in energy. On the other hand, and as expected, all the resonance parameters show a sizable correlation with the normalization and background parameters.

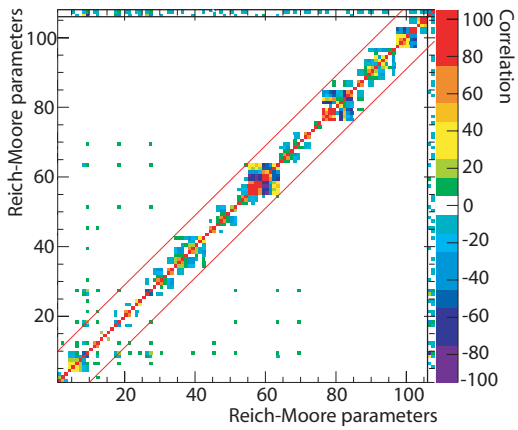

FIG. 8. (Color online) Correlation matrix for the first 35 resonances (E_n, Γ_γ, and Γ_n for each resonance) including the negative resonance (first three parameters) and the normalization and constant background variables (parameters 106 and 107, respectively).

C. Results above 43 eV

Above a few tens of eV the resonances are overlapping strongly and the resonance analysis becomes sensitive mainly to the integral of the resonances and not so much to their shape. In the analysis the value $\Gamma_\gamma = 40.9(18)$ meV was kept fixed for all resonances and thus only the energy and neutron width, as well as the normalization and background parameters, have been fitted in the region between 43 and 500 eV. This energy interval contains a total of 583 resonances and thus it was divided in 10 smaller intervals. The analysis of such intervals reduces computing time and, more important, allows testing the consistency of the correction parameters (normalization and background) as a function of the neutron energy. In the range between 120 and 140 eV and 310–370 eV only the capture yield was analyzed because several black filters were used in the transmission experiment in these regions. In those cases the normalization and background have been fixed to the value interpolated from the results of the neighboring energy intervals.

Figures 9 and 10 display the experimental capture yield and the transmission for the lowest and highest intervals between 43 and 500 eV. Again, it is observed that the capture and transmission data are compatible with each other in the complete energy range, meaning that they can be both reproduced from a single set of resonance parameters using a fixed value of the radiative width.

D. Fitted values of the normalization and background

The analysis of each of the 10 energy intervals provides an independent value of the normalization factor and the

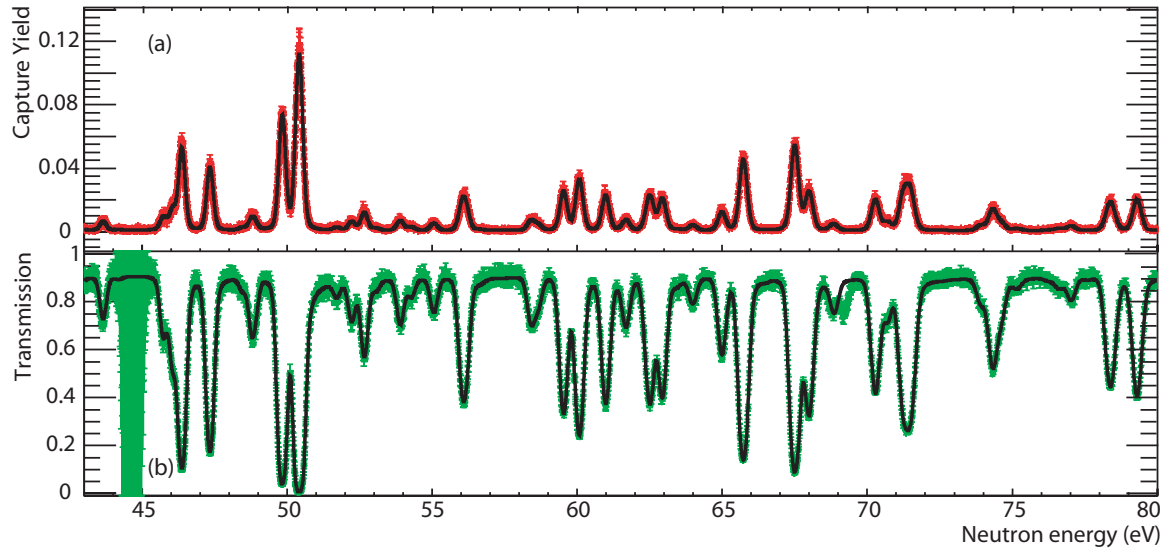

FIG. 9. (Color online) SAMMY fits (solid lines) to the capture yield (red markers) and the transmission (green markers) data between 43 and 80 eV.

background level and hence it is important to confirm that all the values are consistent.

The values of the background found in each interval are given in Table IV, where it is observed that the background level decreases from 3×10^{-4} at 1 eV to 0.8×10^{-4} at 500 eV. This corresponds to a contribution lower than ∼2% to the capture yield below the resonances and up to 10% in the valleys, which is compatible with the measured values.

The normalization values found in the analysis of each of the energy intervals are shown in Fig. 11. The values are constant within the 2% uncertainty in the energy dependence of the neutron flux with the only exception of the value between 370 and 430 eV. This constant behavior indicates again that the capture and transmission data are compatible at all energies. The reasons behind the slightly larger 5% difference found between 370 and 430 eV have not been identified. It has, however, been discarded that this is related to the existence of large fission or scattering resonance clusters.

E. Statistical properties of the resonance parameters in the RRR

The study of the statistical properties of the resonance parameters is crucial for testing the reliability of the complete set of parameters and also for the calculation of average resonance parameters that serve as input for cross-section calculation models in the unresolved resonance region (Hauser-Feshbach)

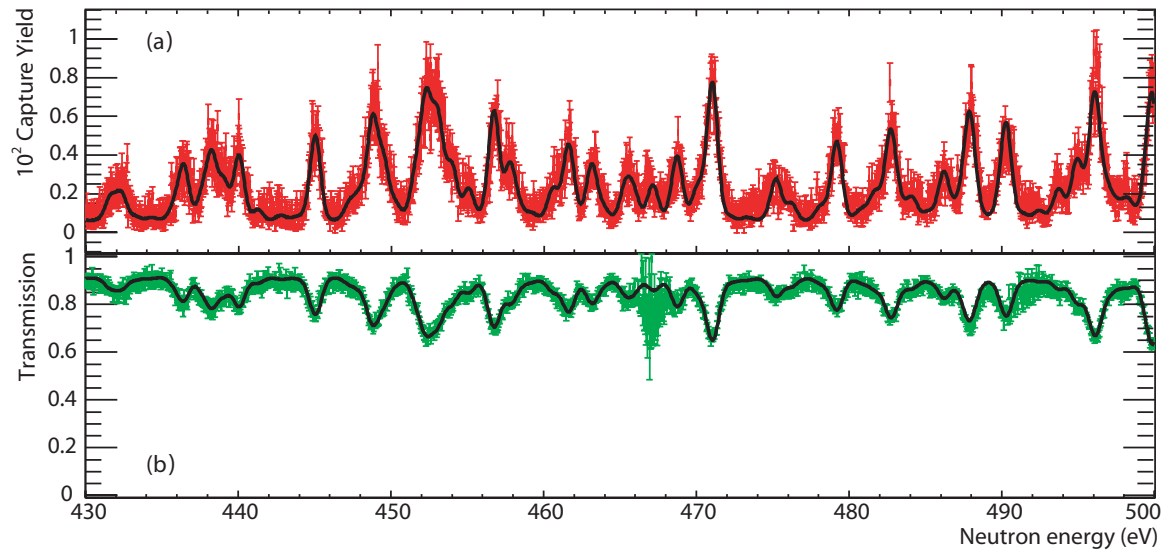

FIG. 10. (Color online) SAMMY fits (solid lines) to the capture yield (red markers) and the transmission (green markers) data between 430 and 500 eV.

TABLE IV. Background level, in units of yield, fitted between 1 and 500 eV. The uncertainty in the background given by SAMMY is lower than a unit in the last digit.

E_n(eV)	Background	E_n(eV)	Background
1–20	0.00031	140–225	0.00015
20–43	0.00029	225–310	0.00011
43–80	0.00021	310–370	0.00010
80–120	0.00018	370–430	0.00010
120–140	0.00016	430–500	0.00008

and at higher energies (pptical model). The level spacing, strength function, and average radiation width are discussed in the following:

(i) *Level spacing*. The cumulative number of resonances as a function of energy shown in Fig. 12 indicates that a significant number of resonances are missing above 150 eV because of the strong overlapping. Below this limit the average level spacing was calculated as a linear fit yielding $\langle D_0 \rangle = 0.56(2)$ eV. The consistency in the distribution of experimental level spacing for each spin is tested by comparison with the expected theoretical Wigner distributions shown in Fig. 14, where the agreement for $J = 3$ (b) resonances is slightly better than that for $J = 2$ (b).

(ii) *Strength function*. The strength function was calculated as the slope of the cumulative sum of reduced neutron widths (see Fig. 13). The resulting value is $S_0(10^{-4}) = 0.98(9)$, where the uncertainty is given by

$$\sigma = \sqrt{\frac{2}{\Delta E} \sum_j g_j^2 D_j}. \tag{3}$$

(iii) *Radiative width*. As mentioned in Sec. IV B, the average radiative width was calculated from all resonances below 43 eV, yielding the value $\langle \Gamma_\gamma \rangle = 40.9(18)$ meV.

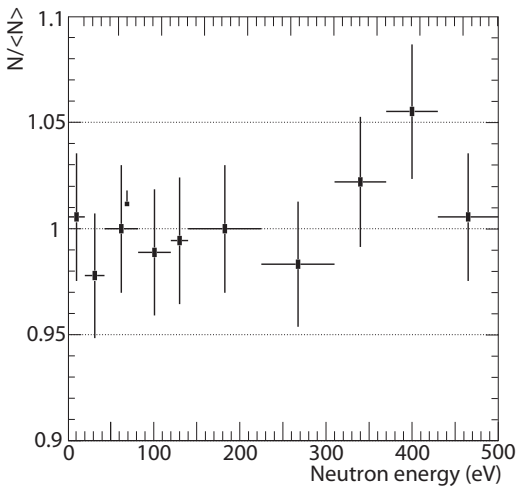

FIG. 11. Variation around the mean value of the normalization found in the different energy intervals.

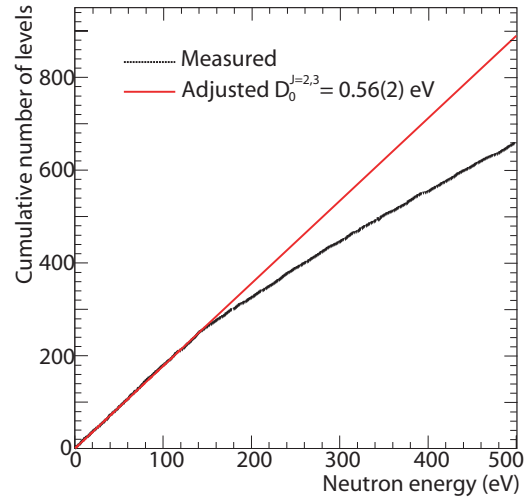

FIG. 12. (Color online) Cumulative number of levels as a function of neutron energy. Both $J = 2$ and $J = -3$ resonances are included.

V. COMPARISON WITH EVALUATIONS AND EXPERIMENTS

A. Average capture cross section

The result of the analysis between 1 and 500 eV is a complete set of resonance parameters for 657 resonances, which shall be available in EXFOR [53]. Because of the large number of resonances and the overlap between them from the small level spacing, the results are better understood in terms of average quantities. In particular, the results have been compared to previous measurements and evaluations by looking at the average cross section $\langle \sigma_\gamma \rangle$ in different energy intervals, calculated with NJOY-99 [54] as

$$\langle \sigma_\gamma \rangle_{i,f} = \frac{\int_{E_i}^{E_f} \sigma_\gamma dE}{E_f - E_i}. \tag{4}$$

Other authors have compared their results in selected energy intervals below 100 eV [8,10] and thus the same intervals

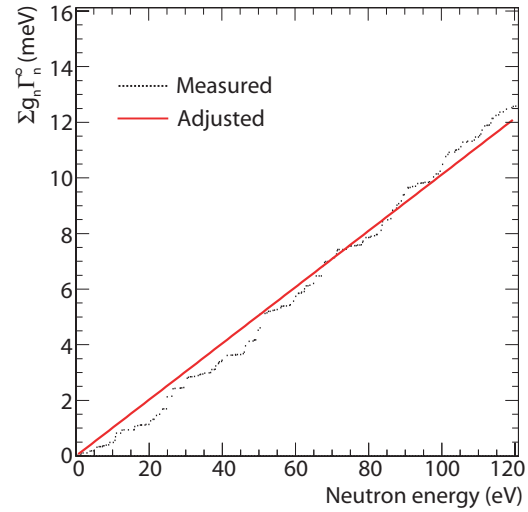

FIG. 13. (Color online) Cumulative sum of reduced neutron widths $\Gamma_n^0 = \Gamma_n(1 \text{ eV}/E_n)^{1/2}$.

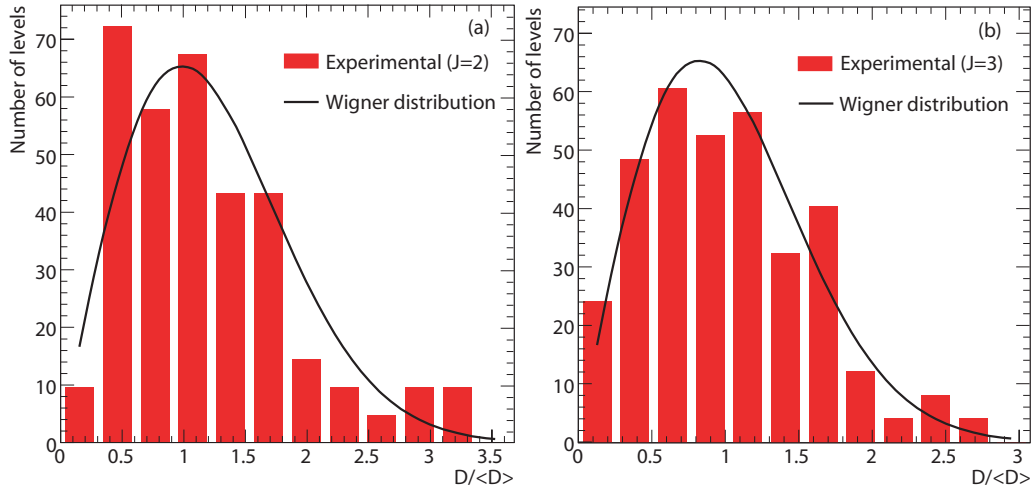

FIG. 14. (Color online) Level spacing distribution of the n_TOF resonance parameters below 90 eV compared to the expected Wigner distribution.

have been chosen in this work. However, the good energy resolution of the n_TOF data allow investigating the average cross sections calculated from resonance parameters up to higher neutron energies and therefore two additional energy intervals have been included: 100–280 eV and 280–500 eV.

The average cross-section values of this work and their comparison with the values from previous measurements and evaluations are summarized in Table V, where the values in bold indicate that the difference found is beyond the uncertainty of our results (3.7%). The experimental values in Table V correspond to the measurements of Hoffman *et al*. [6], Weston and Todd [8], Kobayashi *et al*. [9], and Scherbakov *et al*. [10]. For the sake of clarity, the ratios reported in the table are illustrated in Fig. 15, where only the ratio values between 0.8 and 1.2 have been considered.

The comparison indicates that the evaluated cross sections, as well as the data by Weston and Scherbakov, are in good agreement (1%–4%) with the results of this work. On the contrary, the data of Kobayashi and Hoffman are in clear

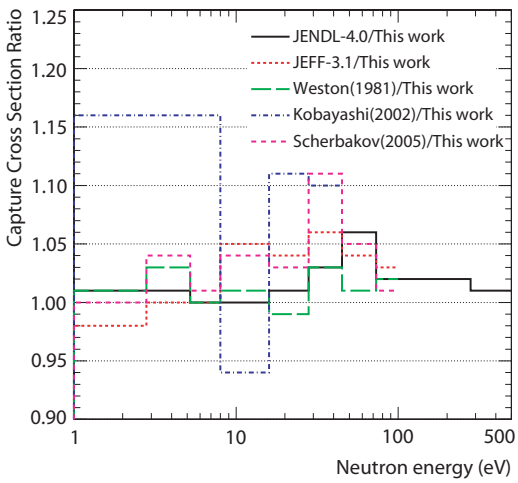

FIG. 15. (Color online) Ratios of the n_TOF average capture cross section of ^{237}Np from 1 to 500 eV and those of previous measurements and evaluations (see Table V).

disagreement in most of the resolved resonance region. In particular,

(i) The results of this work and the evaluated cross sections are in agreement within a few percent (1.7% on average) in the complete resolved resonance region. The most recent ^{237}Np evaluation, JENDL-4.1, is always equal to or larger than n_TOF with maximum differences of 3%, except between 45 and 73 eV where the difference is 6%. In the case of JEFF-3.1 and ENDF/B-VII.1, which date back to 1980, they are 3% higher than the present n_TOF results, being differences larger than 4% (but always smaller than 6%) in some energy regions.

(ii) The data of Hoffman *et al*., available only above 16 eV, are in clear disagreement with this work. In the complete energy range they are between 40% and 50% lower than the present values and hence they are not displayed in Fig. 15.

(iii) The data of Weston and Todd, which allow resolving resonances only below 100 eV, are in good agreement (1.2% higher on average) with this work, showing differences always smaller than 3%.

(iv) The data of Kobayashi *et al*. are in clear disagreement with this work. At low energies (1–8 eV) they are 16% larger; between 8 and 16 eV they are 11% lower; and at higher energies they are always larger, with differences up to 53%.

(v) The data of Scherbakov *et al*., which extend only up to 100 eV, are in overall agreement with the present results except in the energy interval between 28 and 45 eV where they are 11% larger. Other than that, the differences with this work are always lower than 5%, being on average 2.6% larger than the present data.

Although the comparison with evaluations and previous data was made in the form of the cross section integrated over wide energy intervals, it must be emphasized that it is more accurate to measure and analyze high-resolution data (as in the present work), where the resonances can be analyzed individually even if there is a significant overlap. This is related

TABLE V. Average capture cross section of ^{237}Np from 1 to 500 eV calculated with NJOY-99 and compared to the values from previous measurements and evaluations. The values in bold indicate that the difference is beyond the uncertainty in the present results (<4%).

E_1-E_2	$\langle\sigma_\gamma\rangle_{\text{Thiswork}}$	Capture cross-section ratios					
(eV)	(barns)	JENDL−4.0 / Thiswork	JEFF−3.1 [a] / Thiswork	Hoffman / Thiswork	Weston / Thiswork	Kobayashi / Thiswork	Scherbakov / Thiswork
1–2.8	159	1.01	0.98	–	1.01	**1.16**	1.00
2.8–5.2	66.9	1.01	1.0	–	1.03	**1.16**	**1.04**
5.2–8	105	1.00	1.0	–	1.00	**1.16**	1.01
8–16	91.5	1.00	**1.05**	–	1.01	**0.94**	**1.04**
16–28	97.9	1.01	**1.04**	**0.442**	0.99	**1.11**	1.03
28–45	46.0	1.03	**1.06**	**0.554**	1.03	**1.10**	**1.11**
45–73	66.8	**1.06**	**1.04**	**0.492**	1.01	**1.37**	**1.05**
73–100	43.3	1.02	1.03	**0.546**	1.02	**1.53**	1.01
100–280	27.4	1.02		**0.599**	–	–	–
280–500	16.9	1.01		**0.498**	–	–	–
1–500		1.02(2)	1.03(3)	0.52(6)	1.01(1)	1.19(18)	1.04(3)

[a]ENDF/B-VII.1 is similar to JEFF-3.1.

to the fact that the uncertainty caused by the background is minimized in the analysis of resonances with respect to the analysis of average cross sections, where a very accurate determination of the background is crucial.

B. Average resonance parameters

The average parameters resulting from the statistical analysis of the resonance parameters of the SAMMY fits are compared to those from the recommended evaluations and the results of Noguere in Table VI. In all cases, the values from this work are in agreement within uncertainties with those from the recommended evaluations and also with those of the RIPL-2 library. The agreement with the results of Noguere is not as good, being the differences found for all parameters at the very limit with respect to the stated uncertainties.

VI. CONCLUSIONS

The neutron capture cross section of ^{237}Np was measured at n_TOF using the segmented BaF_2 Total Absorption Calorimeter in the energy range between 1 and 500 eV. The combination of the large flight path at n_TOF and the high efficiency of the total absorption calorimeter have provided, with good statistics, the best resolved ^{237}Np(n,γ) cross-section data up to date.

TABLE VI. Average resonance parameters of ^{237}Np determined in this work compared to the values in the evaluations and recommendation libraries.

	This work	JEFF-3.1 JENDL-4.0 ENDF/B-VII.1	RIPL-2	Noguere
D_0 (eV)	0.56(2)	0.58	0.57(3)	0.60(3)
$\langle\Gamma_\gamma\rangle$ (meV)	40.9(18)	40.0	40.8(12)	39.3(10)
$10^4 S_0$	0.98(9)	1.0	0.97(7)	1.02(14)
R' (fm)	10.2(4)	10.5	–	9.8(1)

Along the data reduction process all sources of systematic uncertainty have been carefully investigated. The uncertainties reported are realistic and provide confidence in the overall accuracy of the capture yield (∼5%). The measured capture yield was analyzed with SAMMY individually and in combination with the most reliable transmission data available to date, which have been shown to be in good agreement with the n_TOF capture data in the complete energy range under study. The combination of capture and transmission data yields a capture cross section with an uncertainty better than 4%. The resonance analysis with SAMMY has resulted in a complete set of resonance parameters, the associated covariance matrix, and a set of average (or statistical) parameters suitable for the calculation of cross sections at higher neutron energies.

The compatibility with the transmission data and the agreement with the evaluated capture cross sections indicate that the uncertainty of 15% in the capture cross section of ^{237}Np estimated previous to this work is significantly overestimated. A value of ∼3%–4% in the energy region measured at n_TOF seems more reasonable in the view of the present results and the small differences found with respect to the evaluations (2%–3%) and the capture data from Weston and Todd (1%) and Scherbakov *et al*. (2.6% if the range 28–45 eV is excluded and 3.6% otherwise).

ACKNOWLEDGMENTS

This work was supported partially by the NTOF-ND-XADS project from the European Union 5$^{\text{th}}$ Framework Programme, the IP-EUROTRANS project, the CIEMAT-ENRESA Agreement on the Separación y Transmutación de Residuos Radiactivos, the Spanish Plan Nacional de Física de Partículas under Contract No. FPA2005-06918-C03-01, and the Spanish Consolider Project CPAN Ingenio-2010. The authors thank N. M. Larson (ORNL, USA), G. Noguere (CEA, France), and H. Derrien (ORNL, USA) for their advice on the use of SAMMY and their valuable comments when performing the resonance analysis. This work is part of the Ph.D. thesis of C. Guerrero presented at the Universidad Complutense de Madrid in 2008.

[1] NEA/WPEC-26, *Uncertainty and Target Accuracy Assessment for Innovative Systems using Recent Covariance Evaluations*, NEA/WPEC report, 2008.

[2] NEA Nuclear Data High Priority Request List, http://www.nea.fr/dbdata/hprl/index.html.

[3] A. J. Koning *et al.*, *CANDIDE: Nuclear Data for Sustainable Nuclear Energy*, EUR 23977 EN-2009 report, 2009.

[4] Evaluated Nuclear Data Files at the IAEA, http://www-nds.iaea.org/.

[5] M. S. Smith *et al.*, Phys. Rev. **107**, 525 (1957).

[6] M. M. Hoffman, W. M. Sanders, and M. D. Semon, Bull. Am. Phys. Soc. **21**, 665 (1976).

[7] L. Mewissen, F. Poortmans, I. Cornells, G. Vanpraet, A. Angeletti, G. Rohr, and H. Weigman, Nucl. Sci. Eng. **70**, 155 (1979).

[8] L. W. Weston and J. H. Todd, Nucl. Sci. Eng. **79**, 184 (1981).

[9] K. Kobayashi *et al.*, J. Nucl. Sci. Technol. **39**, 111 (2002).

[10] O. Shcherbakov, K. Furutaka, S. Nakamura, H. Sakane, H. Harada *et al.*, J. Nucl. Sci. Technol. **42**, 135 (2005).

[11] E. I. Esch *et al.*, Phys. Rev. C **77**, 034309 (2008).

[12] D. Paya, Ph.D. thesis, Universite de Paris-Sud, 1972.

[13] G. F. Auchampaugh *et al.*, Phys. Rev. C **29**, 174 (1984).

[14] V. Gressier, Ph.D thesis, University of Paris XI Orsay, 1999.

[15] G. Noguere, Phys. Rev. C **81**, 044607 (2010).

[16] C. Guerrero *et al.*, Nucl. Instrum. Methods A **608**, 424 (2009).

[17] C. Paradela *et al.*, Phys. Rev. C **82**, 034601 (2010).

[18] U. Abbondanno *et al.*, *n_TOF Performance Report*, CERN/INTC-O-011, INTC-2002-037 report, 2002.

[19] F. Gunsing *et al.*, Nucl. Instrum. Methods B **261**, 925 (2007).

[20] J. Pancin *et al.*, Nucl. Instrum. Methods A **524**, 102 (2004).

[21] N. Colonna *et al.*, Energy Environ. Sci. **3**, 1910 (2010).

[22] U. Abbondanno *et al.*, Phys. Rev. Lett. **93**, 161103 (2004).

[23] G. Aerts *et al.*, Phys. Rev. C **73**, 054610 (2006).

[24] C. Domingo-Pardo *et al.*, Phys. Rev. C **74**, 025807 (2006).

[25] M. Calviani *et al.* (n_TOF Collaboration), Phys. Rev. C **80**, 044604 (2009).

[26] R. Plag *et al.*, Nucl. Instrum. Methods A **496**, 425 (2003).

[27] S. Marrone *et al.*, Nucl. Instrum. Methods A **490**, 299 (2002).

[28] U. Abbondanno *et al.*, Nucl. Instrum. Methods A **521**, 454 (2004).

[29] U. Abbondanno *et al.*, Nucl. Instrum. Methods A **538**, 692 (2005).

[30] C. Guerrero *et al.* (unpublished).

[31] E. Mendoza *et al.*, J. Korean Phys. Soc. **59**, 1813 (2011).

[32] C. Guerrero *et al.*, Nucl. Instrum. Methods A **671**, 108 (2012).

[33] S. Agostinelli *et al.*, Nucl. Instrum. Methods A **506**, 250 (2003).

[34] Institute for Physics and Power Engineering, Obnisk (Russia), www.ippe.obnisk.ru.

[35] E. Berthoumieux, *Preliminary Report on BaF_2 Total Absorption Calorimeter Test Measurement*, Rap. Tech., CEA-Saclay/DAPNIA/SPhN report, 2004.

[36] J. L. Tain and D. Cano-Ott, Nucl. Instrum. Methods A **571**, 719 (2007).

[37] C. Guerrero *et al.*, J. Korean Phys. Soc. **59**, 1510 (2011).

[38] C. Borcea *et al.*, *Results from the Commissioning of the n TOF Spallation Neutron Source at CERN*, CERN-SL-2002-051 report, 2002.

[39] R. Macklin, J. Halperin, and R. Winters, Nucl. Instrum. Methods A **164**, 213 (1979).

[40] O. Bouland, H. Derrien, N. M. Larson, and L. C. Leal, Nucl. Sci. Eng. **127**, 105 (1997).

[41] N. M. Larsson, *Updated Users' Guide for SAMMY: Multilevel R-matrix Fits to Neutron Data Using Bayes' Equations*, ORNL/TM-9179/R7 report, 2006.

[42] C. Coceva *et al.*, Nucl. Instrum. Methods A **489**, 346 (2002).

[43] D. Bernard and A. Santamarina, *^{237}Np XS Experimental Validation. Proposal for JEFF3 Modification*, JEF/DOC-1144 report, 2006.

[44] G. Noguere, D. Bernard, and C. De Saint-Jean, *Multi-group Covariance Matrix for the Resolved Resonance Range of Np-237*, JEF/DOC-1174 report, 2007.

[45] C. E. Thomas and R. G. Thomas, Phys. Rev. **104**, 483 (1956).

[46] A. Courcelle, G. Noguere, and N. M. Larson, *Experimental Tests of the Crystal Lattice Model of the R-Matrix Code* SAMMY, JEFDOC-980 report, 2003.

[47] V. Gressier, D. G. Naberejnev, and C. Mounier, Annals of Nuclear Energy **27**, 1115 (2000).

[48] T. Belgya *et al.*, *Handbook for Calculations of Nuclear Reaction Data (RIPL-2)*, IAEA-TECDOC-1506 report, 2006.

[49] F. H. Fröhner, computer code SESH, Gulf General Atomic, report No. GA-8330, 1968.

[50] F. H. Fröhner, B. Goel, and U. Fischer, computer code FITACS, Argonne National Laboratory Report No. ANL-83-4, Argonne, IL, 1983.

[51] F. H. Frohner, Nucl. Sci. Eng. **103**, 119 (1989).

[52] W. Hauser and H. Feshbach, Phys. Rev. **87**, 366 (1952).

[53] Experimental Nuclear Reaction Data (EXFOR), www-nds.iaea.org/exfor/.

[54] The NJOY Nuclear Data Processing System (Version 91), Los Alamos National Laboratory Report No. LA-12740-M, Los Alamos, NM, 1994.